000
001
002
003
004
005
006
007
008
009
010
011
012
013
014
015
016
017
018
019
020
021
022
023
024
025
026
027
028
029
030
031
032
033
034
035
036
037
038
039
040
041
042
043
044
045
046
047
048
049
050
051
052
053

DEEPGATE4: EFFICIENT AND EFFECTIVE REPRESENTATION LEARNING FOR CIRCUIT DESIGN AT SCALE

Anonymous authors
Paper under double-blind review

ABSTRACT

Circuit representation learning has become pivotal in electronic design automation, enabling critical tasks such as testability analysis, logic reasoning, power estimation, and SAT solving. However, existing models face significant challenges in scaling to large circuits due to limitations like over-squashing in graph neural networks and the quadratic complexity of transformer-based models. To address these issues, we introduce **DeepGate4**, a scalable and efficient graph transformer specifically designed for large-scale circuits. DeepGate4 incorporates several key innovations: (1) an update strategy tailored for circuit graphs, which reduce memory complexity to sub-linear and is adaptable to any graph transformer; (2) a GAT-based sparse transformer with global and local structural encodings for AIGs; and (3) an inference acceleration CUDA kernel that fully exploit the unique sparsity patterns of AIGs. Our extensive experiments on the ITC99 and EPFL benchmarks show that DeepGate4 significantly surpasses state-of-the-art methods, achieving 15.5% and 31.1% performance improvements over the next-best models. Furthermore, the Fused-DeepGate4 variant reduces runtime by 35.1% and memory usage by 46.8%, making it highly efficient for large-scale circuit analysis. These results demonstrate the potential of DeepGate4 to handle complex EDA tasks while offering superior scalability and efficiency.

1 INTRODUCTION

Circuit representation learning has emerged as a crucial area in electronic design automation (EDA), reflecting the broader trend in AI of learning general representations for diverse downstream tasks, such as testability analysis (Shi et al., 2022), logic reasoning (Deng et al., 2024; Wu et al., 2023), power estimation (Khan et al., 2023), and SAT solving (Li et al., 2023; Shi et al., 2024a). In this domain, the DeepGate family (Li et al., 2022; Shi et al., 2023) emerges as pioneering approaches, formulating circuit netlists into graphs and utilizing graph neural networks (GNNs) to learn gate-level embeddings. DeepGate (Li et al., 2022) converts arbitrary circuit netlists into And-Inverter Graphs (AIGs) and uses logic-1 probabilities from random simulations for model supervision. Its successor, DeepGate2 (Shi et al., 2023), improves on this by learning disentangled structural and functional embeddings. In addition to the DeepGate Family, Gamora (Wu et al., 2023) extends reasoning capabilities by representing both logic gates and cones, while HOGA (Deng et al., 2024) enhances the scalability and generalizability of GNNs through hop-wise aggregation.

Despite the success on tiny circuits, inherent limitations of the GNN-based framework persist when it scales to large circuits, including difficulty in capturing long-range dependencies (Alon & Yahav, 2020), susceptibility to over-smoothing (Akansha, 2023) and over-squashing (Rusch et al., 2023), which results in poor performance on complex circuits. Consequently, DeepGate3 (Shi et al., 2024b) draws inspiration from transformer-based graph learning models by tokenizing circuits into sequences and employing graph transformers to capture global relationships within DAG-based structures. While DeepGate3 introduces fine-tuning strategies for scaling from smaller to larger circuits, it still struggles to handle circuits with millions of gates due to the significant memory overhead and computation redundancy of dense transformer blocks. Therefore, training an efficient and effective circuit representation learning model still remains a challenge.

In general domain, previous research on improving model efficiency has shown great potential in scaling GNNs and graph Transformers; however, significant challenges still remain in applying these advancements to circuit representation learning. These models can be broadly categorized

into two types: linear graph transformers and sub-linear GNNs. On the one hand, the linear Graph Transformers, such as GraphGPS (Rampášek et al., 2022), Exphormer (Shirzad et al., 2023), NodeFormer (Wu et al., 2022), DAGformer (Luo et al., 2024), and NAGphormer (Chen et al., 2022), leverage graph sparsity to perform different sparse attention, reducing memory consumption from quadratic to linear. Despite the advancement, training these models on practical circuit designs with millions or billions of gates still suffer from Out-Of-Memory(OOM) error. On the other hand, the sub-linear GNNs, such as GNNAutoScale (Fey et al., 2021), SketchGNN (Ding et al., 2022), and GraphFM (Yu et al., 2022), achieve sub-linear memory complexity by employing historical embeddings during training, with randomly sampled sub-graphs. However, these methods are primarily tailored for undirected graphs and pose challenges when applied to Directed Acyclic Graphs (DAGs). Specifically, sub-linear GNNs with random sampling strategies (Fey et al., 2021; Yu et al., 2022; Ding et al., 2022) disregard the causal relationships between sub-graphs by applying completely random sampling, resulting in suboptimal performance on function-related tasks.

In response to these challenges, we propose **DeepGate4**, an efficient and effective graph transformer specifically designed to scale to large circuits. Building on the architecture of DeepGate3 as illustrated in Figure 1, DeepGate4 utilizes GNN-based tokenizer to encode circuit function and structure. These embeddings are then processed by a transformer for global aggregation. Our approach introduces several key innovations:

- **An updating strategy** tailored for DAGs based on partitioned graph, ensuring that gate embeddings are computed in logical level order, with each gate being processed only once, thus eliminating redundant computations. While DeepGate3 is limited to fine-tuning graphs with up to 50k nodes, the proposed updating strategy, which is adaptable to any graph transformer, achieve sub-linear memory complexity and thus enable efficient training on graphs with millions of nodes.
- **A GAT-based sparse transformer** with global virtual edges, reducing both time and memory complexity to linear in a mini-batch. We further introduce structural encodings for transformers on AIGs by incorporating global and local structural encodings in initialized embedding.
- **An inference acceleration kernel**, Fused-DeepGate4, designed to optimize the inference process of tokenizer and GAT components with well-designed CUDA kernels that fully exploit the unique sparsity patterns of AIGs.

Experimental results on the ITC99 and EPFL benchmarks demonstrate that DeepGate4 significantly outperforms state-of-the-art methods, with improvements of 15.5% and 31.1%, respectively, over the second-best method in overall performance. Furthermore, our Fused-DeepGate4 model, with inference acceleration optimizations, achieves a 41.3% reduction in runtime and 51.3% reduction in memory usage on the ITC99 benchmark, and a 28.2% reduction in runtime and 32.5% reduction in memory usage on the EPFL benchmark. We also evaluate the generalizability of DeepGate4 across circuits of varying scales. DeepGate4 exhibits strong generalizability, delivering outstanding overall performance on circuits with 400K gates, despite being trained on circuits averaging just 15K gates. Moreover, when inference on circuits ranging from 400K gates to 1.6M gates, while GNNs exhibit linear memory growth, our models maintain constant memory usage. These results suggest that DeepGate4 has the potential to scale both effectively and efficiently to circuits with millions, even billions of gates.

2 Related Work

Circuit Representation Learning Circuit representation learning has become a pivotal area in electronic design automation (EDA), reflecting the broader trend in AI of learning general representations for diverse downstream tasks. In this domain, the DeepGate family (Li et al., 2022; Shi et al., 2023) emerges as pioneering approaches, exploring GNNs to encode AIGs and enabling support for a variety of EDA tasks such as testability analysis (Shi et al., 2022), power estimation (Khan et al., 2023), and SAT solving (Li et al., 2023; Shi et al., 2024a). The Gamora (Wu et al., 2023) and HOGA (Deng et al., 2024) further extend reasoning capabilities by representing both logic gates and cones. PolarGate (Liu et al., 2024) seeks to overcome functionality representation bottlenecks by leveraging ambipolar state principles.

Considering the inherent limitation of GNNs, e.g. over-squashing or over-smoothing, recent work DeepGate3 (Shi et al., 2024b), as illustrated in Figure 1, utilizes DeepGate2 as a tokenizer and then leverages the global aggregation mechanism of transformers with a connective mask to enhance circuit representation. However, new challenges arise when scaling to large AIGs: transformer-based models suffer from quadratic complexity, making training on large AIGs impractical.

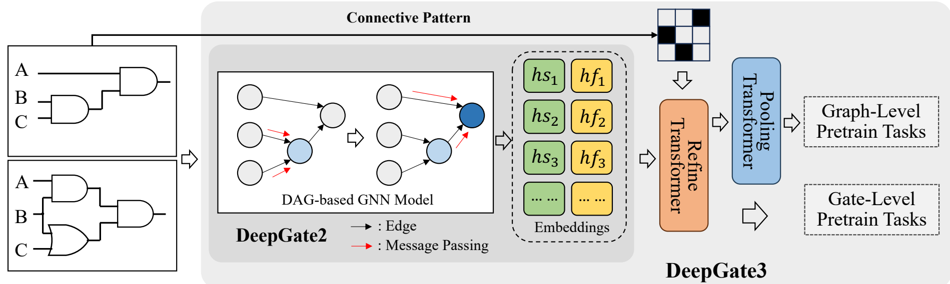

Figure 1: The overview of DeepGate2 and DeepGate3

Advances and Challenges in Graph Transformers and Sub-Linear GNNs for Large-Scale Circuits Graph transformer models typically operate on fully-connected graphs, where every pair of nodes is connected, regardless of the original graph's structure. SAN (Kreuzer et al., 2021), Graphormer (Ying et al., 2021), GraphiT (Mialon et al., 2021), and GraphGPS (Rampášek et al., 2022) apply dense attention mechanisms with various positional and structural encodings. While these methods deliver outstanding performance, the quadratic complexity makes them impractical for large graphs. Recent approaches, such as Exphormer (Shirzad et al., 2023), Nodeformer (Wu et al., 2022), NAGformer (Chen et al., 2022), and DAGformer (Luo et al., 2024), leverage the sparse patterns of graphs to employ sparse transformers, reducing complexity to linear. However, even with these improvements, applying them to circuits with millions of gates remains challenging.

Sub-linear GNNs, such as GNNAutoScale (Fey et al., 2021) and SketchGNN (Ding et al., 2022) tackle this issue by incorporating historical embeddings during training, reducing memory complexity by reusing embeddings from prior iterations. This allows for constant GPU memory consumption relative to graph size. GraphFM (Yu et al., 2022) improves the historical embeddings updating by introducing feature momentum. However, applying them to AIGs remains challenging since they disregard the causal relationships between sub-graphs by applying completely random sampling. Specifically, when modeling circuit functionality as a computational graph, it is essential to follow a strict topological order, reasoning from primary inputs (PIs) to primary outputs (POs) based on logic levels (Li et al., 2022).

The Necessity of System-Level GNN Optimizations for Circuit Processing System-level optimization of GNNs aims to reduce memory consumption and accelerate inference and training time, thereby improving the efficiency of GNN execution. Single GPU systems primarily optimize through operator reorganization, operator fusion, and data flow optimization. FuseGNN (Chen et al., 2020) accelerates the computation process by fusing any two edge-centric operators and storing intermediate data from the forward pass. However, it still consumes a large amount of memory. Fused-GAT (Zhang et al., 2022), recognized as the state-of-the-art approach, reduces redundant computations by postponing the propagation operator. It has been widely adopted in PyTorch Geometric (PyG) (PyG, 2024) implementations of the GAT network (e.g., GATConv, FuseGATConv), and its fused operators and recomputation strategy significantly reduce the memory required for execution. However, existing GNN acceleration techniques, such as Fused-GAT, were primarily designed for social network and citation network datasets, where the node degree follows a power-law distribution (Eikmeier & Gleich, 2017). In contrast, AIGs exhibit a uniform node degree distribution and have significantly fewer edges (1 or 2 edges per node). Consequently, these methods perform suboptimally on AIG graphs due to imbalanced workload and substantial synchronization overhead.

3 METHOD

3.1 OVERVIEW

The overall pipeline of our method is illustrated in Figure 2. The core idea of our method is to partition a large graph into small cones and encode these cones level by level, enabling the training of a graph transformer with sub-linear memory complexity. Section 3.2 details the graph partitioning process. Section 3.3 discusses our observations on overlap regions, and based on these observations, we propose the updating strategy in Section 3.4. In Section 3.5, we show the model architecture and structural encoding of our sparse transformer. Section 3.6 introduces our training objectives and a multi-task loss balancer that adjusts the weight of each component. Finally, Section 3.7 introduces inference optimization techniques to further reduce the inference runtime and memory usage.

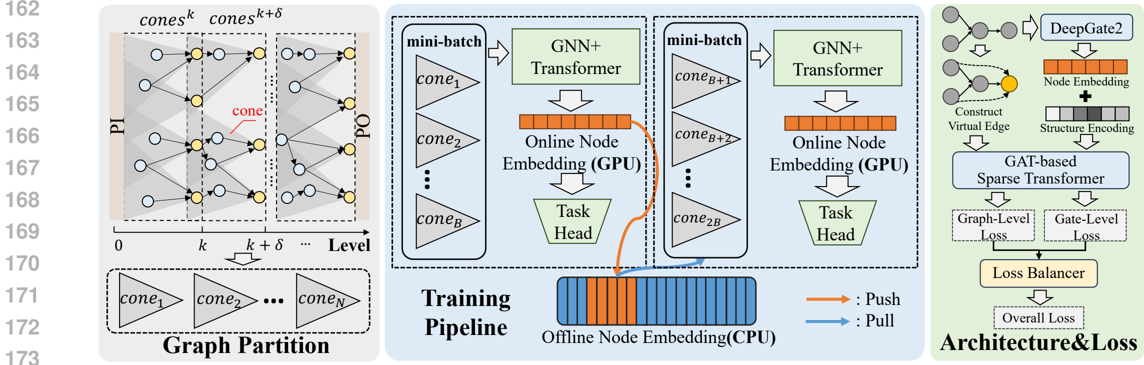

Figure 2: The overall pipeline of our method. In our training pipeline, the embedding exchanging is implemented through the following two operations: **Push(GPU to CPU)**: After encoding a mini-batch, the online node embeddings are saved in offline historical embedding. **Pull(CPU to GPU)**: Before encoding a mini-batch, the offline historical embeddings are used to initialize the online node embeddings in the overlap region.

3.2 Graph Partition

Given an AIG $\mathcal{G} = (V, E)$, with node set V, and edge set $E \subseteq V \times V$, the AIG contains three type of nodes: primary input(PI), AND gate and NOT gate. The gate type can be easily identified by its in-degree: the in-degree of a PI is 0, the in-degree of an AND gate is 2, and the in-degree of a NOT gate is 1. We first compute the logic level of each gate in topological order according to the following equation:

$$level(v) = \begin{cases} 0 & \text{if } v \text{ is a PI} \\ 1 + \max\limits_{(u,v)\in E} level(u) & \text{otherwise} \end{cases} \tag{1}$$

For an AIG, we define a partial order $\preccurlyeq_k$ that $u \preccurlyeq_k v$ if there exists a path from u to v with length less than or equal to k. Given a node $v \in V$, based on the partial order $\preccurlyeq_k$, we define a cone by $\mathbf{cone_k}(v) = \{u \in V : u \preccurlyeq_k v\}$. Since the maximum in-degree of any node in an AIG is 2, the maximum size of $\mathbf{cone_k}(v)$ is $2^{k+1} - 1$.

As illustrated in Figure 2, given an AIG $\mathcal{G} = (V, E)$, with cone depth k and stride $\delta < k$, we define the graph partition by Algorithm 1. Initially, we focus on gathering all the $cone_i^k$ that terminate at logic level k. Moving forward with stride δ, we continue collecting with output gates situated at level $k+\delta$. Note that the chosen value of δ is smaller than k in order to guarantee an overlap between cones in different level. The aforementioned process is repeated iteratively until the partitioned areas cover the entire circuit.

3.3 Observation and Motivation

For Intra-Level overlap, i.e. $cone_i^l \cap cone_j^l$, as shown in Figure 3a, note that if a gate v is in the overlap region, then all the fan-in nodes of v must be in the overlap region. Specifically, if $v \in cone_i^l \cap cone_j^l$, then $\forall u \in \{u \in cones^l : u \preccurlyeq_k v\}$, we have $u \in cone_i^l \cap cone_j^l$, since v share the same fan-in region in both $cone_i^l$ and $cone_j^l$. This implies that when computing the embedding of a gate within the overlap region from scratch, the receptive field remains unchanged. When inference, since both the initialization method and model parameters are consistent, the embedding of these gates will be identical across different mini-batches.

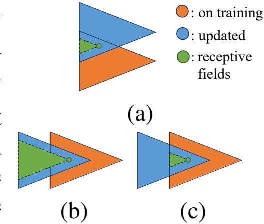

Figure 3: Observation.

For Inter-Level overlap, i.e. $cones^{l-\delta} \cap cones^l$, as illustrated in Figure 3b and Figure 3c, assume that we $v \in cones^{l-\delta} \cap cones^l$, we can define the receptive fields at different levels as follows: $R_{l-\delta}(v) = \{u \in cones^{l-\delta} : u \preccurlyeq_k v\}$ and $R_l(v) = \{u \in cones^l : u \preccurlyeq_k v\}$. According to the definition of $\preccurlyeq_k$, we observe that $R_l(v) \subseteq R_{l-\delta}(v)$, in other words, $R_l(v)$ can be regarded as $R_{l-\delta}(v)$ restricted by $cones^l$. This ensures that using historical embedding of nodes in $cones^{l-\delta}$

216 introduce a larger receptive filed. In contrast, computing the embedding of gate v in $cones^l$ from scratch will restrict the receptive field to the current level, preventing it from capturing long-range dependencies from PIs. The receptive field affects the computations of the GNN tokenizer and sparse transformer, as they aggregate embeddings within the receptive field for node v. Therefore, this limitation on the receptive field will lead to significant estimation errors when performing function-related tasks (Deng et al., 2024; Liu et al., 2024).

Algorithm 1 Graph Partition

Input: AIG $\mathcal{G} = (V, E)$, cone depth k, stride $\delta < k$

1: $L \leftarrow \max_{v \in V} level(v)$, $l \leftarrow k$
2: **while** $l \le L$ **do**
3: $\quad cones^l \leftarrow list()$, $i \leftarrow 0$
4: $\quad$ **for** v in $\{v \in V : level(v) = l\}$ **do**
5: $\quad\quad$ Get sub-graph $cone_i^l \leftarrow \mathbf{cone_k}(v)$
6: $\quad\quad$ Add $cone_i^l$ to $cones^l$, $i \leftarrow i + 1$
7: $\quad$ **end for**
8: $\quad l \leftarrow l + \delta$
9: **end while**
10: **for** v in $\{v \in V : \text{out-degree}(v) = 0\}$ **do**
11: $\quad$ Get sub-graph $g \leftarrow \mathbf{cone_k}(v)$
12: $\quad$ Add g to $cones^{level(v)}$
13: **end for**
14: **return** cones list $[cones^k, cones^{k+\delta}, ...]$

Algorithm 2 Training Pipeline

Input:
cone depth k, stride δ,
partitioned cones $[cones^k, cones^{k+\delta}, ...]$,
mini-batch size B

1: **for** l in $[k, k + \delta, ...]$ **do**
2: $\quad$ **if** $l \ne k$ **then**
3: $\quad\quad$ Inter-Level Updating on $[cones^k, cones^{k+\delta}, ..., cones^l]$
4: $\quad$ **end if**
5: $\quad m \leftarrow len(cones^l)/B$
6: $\quad$ **for** i in range(0,m) **do**
7: $\quad\quad$ sample mini-batch $batch_i^l$ in $cones^l$
8: $\quad\quad$ Intra-Level Updating on $batch_i$
9: $\quad$ **end for**
10: **end for**

3.4 UPDATING STRATEGY

After partition, we get cones with level in $[k, k + \delta, ...]$. As outlined in Algorithm 2, we encode the cones starting from the smaller levels and progressing to the larger ones. Based on the observation in the Section 3.3, we propose Intra-Level Updating for cones at the same level and Inter-Level Updating for cones at different levels. Figure 4 illustrates the detailed updating process when the mini-batch size is 1.

Intra-Level Updating Given a cone list at the same level $cones^l = [cone_1^l, cone_2^l, ..., cone_n^l]$, we divide them into mini-batches $[batch_1^l, batch_2^l, ..., batch_m^l]$. When encoding $batch_i^l$, we first check if the gates in $batch_i^l$ have already been updated in the previous stage. If so, we retrieve their embeddings from the historical embeddings and remove all the in-edges of these gates, ensuring that their embedding will not be updated further in subsequent stages. We then send $batch_i^l$ to the model to compute the embedding of other gates, after which we will store these embedding in historical embedding and mark all the gates in $batch_i^l$ as updated in the following stage.

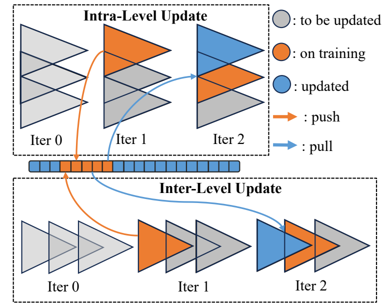

Figure 4: The updating process when the mini-batch size is 1.

Inter-Level Updating Given two lists of cones at different level $cones^{l-\delta}$ and $cones^l$, we ensure that $cones^{l-\delta} \cap cones^l \ne \emptyset$ due to the condition $\delta < k$ in the Algorithm 1. This mechanism allows the message from the previous level to propagate to the current level and ensures that a gate v can acquire the context information from *PIs* to the current gate, i.e. a gate v can aggregate information from $\{u : u \preccurlyeq_\infty v\}$, which is consistent with the information propagation flow in AIGs. The updating method is similar with Intra-Level Updating: given a cone list $cones^l$, for the gates in $cones^{l-\delta} \cap cones^l$, we will retrieve their embedding from historical embedding and remove all the in-edges. For the updating of remaining gates, we leave them for Intra-Level Updating with $cones^l = [cone_1^l, cone_2^l, ..., cone_n^l]$.

3.5 GAT-BASED SPARSE TRANSFORMER

GAT-based Sparse Attention DAGformer (Luo et al., 2024) and DeepGate3 (Shi et al., 2024b) propose to use connective patterns as masks in transformers to effectively restrict attention in DAGs. Inspired by these approaches, we replace the Multi-head Attention module in the Transformer with a GAT module to ensure global aggregation while preserving the original transformer structure, as illustrated in Figure 5. Given a node $v \in cone_i^l$, it should aggregate information from $\{u \in cone_i^l : u \preccurlyeq_k v\}$. To achieve this, we construct virtual edges $\bar{E}$ defined as $\{(u, v) : u \preccurlyeq_k v, u \in cone_i^l\}$, which has similar function to the attention masks in DAGformer and DeepGate3. The original graph, augmented with these virtual edges, i.e. $\bar{\mathcal{G}} = (V, E \cup \bar{E})$, is then passed to the GAT-based sparse transformer to compute the embedding of each node.

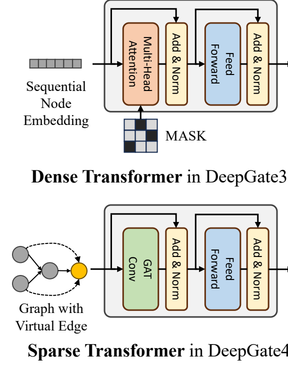

Figure 5: Transformer Architecture

Structural Encoding In a circuit, the structure of a gate is determined by its logic level and connection pattern. Based on the aggregation mechanism of the tokenizer and sparse transformer, a gate can only acquire information from its fan-in region. However, this overlooks the out-edge pattern of a node, which is crucial for timing properties. To enhance the model's ability to capture structural information, we encode the logic level and out-degree of a gate as part of the initial structural embedding. Specifically, for a given node v, the structural encoding is computed by:

$$SE(v) = Emb_l(level(v)) + Emb_{and}(OutAND(v)) + Emb_{not}(OutNOT(v)), \quad (2)$$

where $Emb(\cdot)$ represents a linear layer, and $OutAND(\cdot)$ and $OutNOT(\cdot)$ denote the number of *AND* gates and *NOT* gates in $\{u : v \preccurlyeq_1 u, u \neq v\}$ respectively.

3.6 TRAINING OBJECTIVE

Multi-Task Training During the training phase of DeepGate4, we incorporate both gate-level and graph-level tasks, following the setup in DeepGate3 (Shi et al., 2024b). To separate the functional and structural embeddings, we employ training tasks with distinct labels to supervise each component:

$$L_{func} = L_{gate}^{prob} + L_{gate}^{tt_pair} + L_{graph}^{tt} + L_{graph}^{tt_pair} \quad (3)$$

$$L_{stru} = L_{gate}^{con} + L_{graph}^{size} + L_{graph}^{depth} + L_{graph}^{ged_pair} + L_{in} \quad (4)$$

$$L_{all} = L_{func} + L_{stru} \quad (5)$$

For a detailed explanation of each component, please refer to Section A.2.

Multi-Task Loss Balance To stabilize the training process and balance the weights of each loss, inspired by previous works (Défossez et al., 2022; Chen et al., 2018), we introduce a loss balancer based on the gradient of the final layer of the sparse transformer. Given the last layer's weight w and a loss l_i, we compute the gradient $g_i = \frac{\partial l_i}{\partial w}$. The gradient norm $\|g_i\|_2^\beta$ is computed by exponential moving average of g_i with decay β. The balanced loss of l_i is computed $\tilde{l}_i = \frac{l_i}{\|g_i\|_2^\beta}$ and all components are summed to form the overall loss for training.

3.7 INFERENCE ACCELERATION

Although the graph partitioning method provides the ability to train and infer on arbitrarily large graphs, as the number of nodes increases, the number of partitions also grows, significantly increasing the total computation time. Fused-GAT (Zhang et al., 2022) has already demonstrated excellent results by storing intermediate variables at the node level rather than the edge level, making it particularly effective for graphs with numerous edges. However, applying it directly to our tokenizer, i.e. DeepGate2, presents certain challenges: (1) the GNN component of DeepGate2 uses an aggregation mechanism similar to GAT; however, since the maximum in-degree for each node is 2, applying the Fused-GAT strategy would result in severe thread waste ((32 - 2) / 32 = 93.75%). (2) Fused-GAT calculates the softmax across many edges using the warp-level primitive *shfl_xor_sync* to synchronize the computed sum and max values, introducing substantial synchronization overhead.

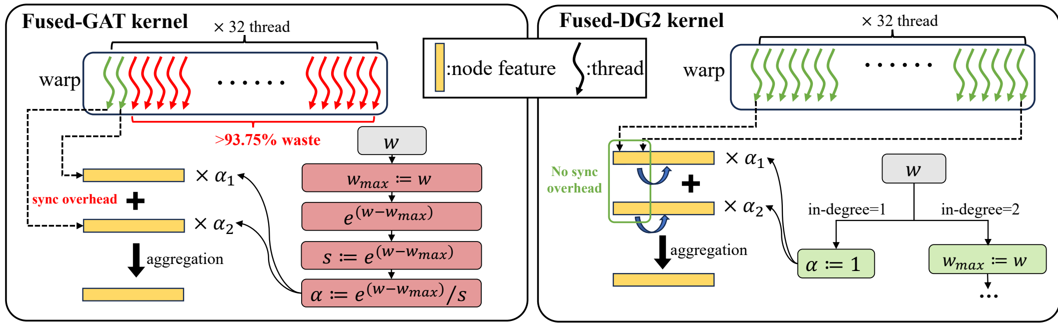

Figure 6: Comparison between Fused-GAT and our Fused-DG2 kernel. **Left**: Fused-GAT suffers from thread waste, unnecessary softmax computation when in-degree is 1, and synchronization overhead for softmax intermediate results between threads; **Right**: Fused-DG2 reallocates thread workloads, with each thread within a warp handling a portion of feature dimensions, avoiding thread waste and eliminating synchronization by independently computing attention scores, significantly reducing computation time. Furthermore, we skip the softmax computations in certain cases.

Efficient workload balance and skip computation. We reassigned the thread computation tasks as Figure 3.7 shows, where each thread is responsible for the aggregation of each node, calculating all α values for incoming edges and performing the multiplication and accumulation, thereby avoiding the high softmax overhead, additionally, due to the characteristics of AIG graphs, where the number of edges is less than twice of nodes, storing intermediate variables at the node level is less efficient than directly storing edge information. Therefore, we switched to performing computations directly on the edges. Finally, we observed that when the in-degree is 1, we can skip the computation entirely, as the softmax result is straightforward, i.e. $\alpha = 1$. By applying these methods, we reduced both the model's inference time and memory consumption.

4 Experiment

4.1 Experiment Setting

Dataset We collect the circuits from various sources, including benchmark netlists in ITC99 (Davidson, 1999) and EPFL (Amarú et al., 2015). All designs are transformed into AIGs by ABC tool (Brayton & Mishchenko, 2010). The statistical details of datasets can be found in Section A.1.

Implementation Details We partition the large circuits into small cones. In Algorithm 1, we set k to 8 and δ to 6. The dimensions of both the structural and functional embedding are set to 128. The depth of Sparse Transformer is 12 and the depth of Pooling Transformer is 2. All training task heads are 3-layer multilayer perceptrons (MLPs). We train all models for 200 epochs to ensure convergence. The training is performed with a batch size of 1 and mini-batch size of 128 on one Nvidia A800 GPU. We utilize the Adam optimizer with a learning rate of 10^{-4}. We report the average performance and standard deviation of the last 5 epochs, and losses without balanced weight.

4.2 Main Result

We compare the performance of our model with other methods on both the ITC99 and EPFL benchmarks. Table 1 presents a detailed comparison of the ITC99 benchmark across various training tasks. GNNs, such as GCN (Kipf & Welling, 2016), GraphSAGE (Hamilton et al., 2017), GAT (Veličković et al., 2017), PNA (Corso et al., 2020), DeepGate2 (Shi et al., 2023), and PolarGate (Liu et al., 2024), consume approximately 30-40 GB of GPU memory when training on ITC99, which has a maximum graph size of 140K gates. This suggests that training GNNs on circuits with more than 500K gates is impractical due to memory constraints. Sparse transformer models, such as GraphGPS (Rampášek et al., 2022), Exphormer (Shirzad et al., 2023), and DAGformer (Luo et al., 2024), also encounter OOM errors when attempting to train on ITC99, despite their linear complexity. However, with our graph partitioning and updating strategy, even dense transformer models like DeepGate3 (Shi et al., 2024b) can be successfully trained on ITC99.

Comparison on Effectiveness In terms of effectiveness, DeepGate4 demonstrates superior results across most training tasks. As shown in Table 3, DeepGate4 achieves state-of-the-art performance on both functional and structural tasks across the ITC99 and EPFL datasets. Regarding overall

Table 1: Detailed comparison experiment on ITC99 benchmark. †We use our graph partition and updating strategy instead of full-batch training.

Model	Training		Gate-level				Graph-level								L_{all}
	Param.	Mem.	L_{gate}^{prob}	$L_{gate}^{tt_pair}$	L_{gate}^{con}	P^{con}	L_{graph}^{tt}	P^{tt}	$L_{graph}^{tt_pair}$	$L_{graph}^{ged_pair}$	L_{graph}^{size}	L_{graph}^{depth}	L_{in}	P^{in}	
GCN	0.76M	31.38G	0.177	0.114	0.616	66.34%	0.589	0.325	0.1596	0.215	2.65	1.0622	1.065	47.93%	6.65
GraphSAGE	0.89M	31.78G	0.115	0.079	0.600	68.33%	0.548	0.290	0.1595	0.203	2.30	0.9628	0.884	51.04%	5.85
GAT	0.76M	34.10G	0.270	0.136	0.605	66.82%	0.588	0.323	0.1601	0.396	5.32	0.8464	0.995	47.94%	9.32
PNA	2.75M	41.99G	0.091	0.079	0.601	68.19%	0.518	0.266	0.1593	0.181	3.50	1.0114	0.810	56.27%	6.95
GraphGPS	6.71M	OOM	-	-	-	-	-	-	-	-	-	-	-	-	-
Exphormer	0.74M	OOM	-	-	-	-	-	-	-	-	-	-	-	-	-
DAGformer	1.90M	OOM	-	-	-	-	-	-	-	-	-	-	-	-	-
DeepGate2	1.28M	32.87G	0.049	0.068	**0.594**	68.77%	0.513	0.274	0.1570	0.238	3.08	0.6772	0.902	48.62%	6.28
DeepGate3	8.17M	OOM	-	-	-	-	-	-	-	-	-	-	-	-	-
PolarGate	0.88M	35.95G	0.226	0.100	0.699	65.92%	0.588	0.326	0.1593	0.237	2.62	0.3705	0.688	52.42%	5.69
HOGA-5	0.78M	42.48G	0.204	0.117	0.609	68.74%	0.493	0.254	0.1624	0.141	3.56	1.1378	0.571	68.99%	6.99
GraphGPS†	6.71M	7.42G	0.109	0.090	0.632	66.11%	0.434	0.178	0.1612	0.195	3.43	0.0061	0.742	54.62%	5.77
Exphormer†	0.74M	6.64G	0.101	0.078	0.674	59.89%	0.349	0.143	0.1160	0.191	2.32	**0.0024**	0.692	59.09%	4.50
DAGformer†	1.90M	9.52G	0.204	0.116	0.660	67.53%	0.540	0.243	0.1749	0.217	4.04	0.3799	0.705	57.99%	7.01
DeepGate3†	8.17M	50.75G	0.055	0.061	0.597	**68.93%**	0.315	**0.133**	**0.0780**	0.125	1.93	0.0030	0.609	68.36%	3.76
DeepGate4	7.37M	7.53G	**0.043**	**0.055**	0.600	67.22%	**0.315**	0.136	0.0803	**0.117**	**1.45**	0.0591	**0.461**	**79.50%**	**3.16**

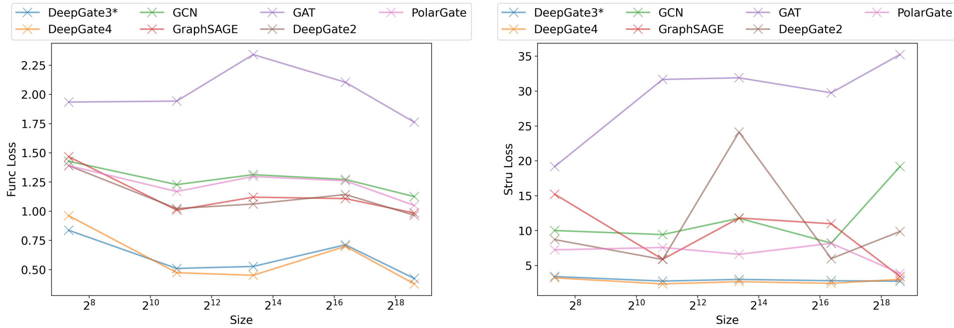

(a) Functional Loss (b) Structural Loss

Figure 7: Performance over different scale circuits.

performance, DeepGate4 reduces the overall loss by 15.5% and 31.1%, respectively, compared to the second-best method. Furthermore, with the proposed structural encoding, DeepGate4 achieves a reduction of 16.4% and 34.9% in structural loss on the ITC99 and EPFL datasets, respectively.

Comparison on Efficiency In terms of efficiency, compared to DeepGate3†, DeepGate4 reduces inference time and memory usage by 77.9% and 92.7% on ITC99, and by 87.8% and 95.2% on EPFL. Furthermore, with our proposed inference optimization, Fused-DeepGate4 (Fused-DG4) reduces inference time and memory usage by 41.4% and 51.4% on ITC99, and by 28.2% and 30.0% on EPFL, compared to DeepGate4.

4.3 Performance over Circuit of Different Scale

In this section, we discuss our model's performance across circuits of varying scales and its generalizability to Out-Of-Distribution (OOD) circuits. We trained our model on the ITC99 dataset, following the split outlined in Table 5. During training, the average graph size is 15k, while for evaluation, we used circuits of different scales, as shown in Table 2.

We extract 128 small circuits from ITC99 to ensure stable evaluation results. The average number of nodes and edges are listed as SMALL (AVG.) in Table 2. B12_OPT_C and B14_OPT_C are the original designs collected from ITC99, while MEM_CTRL is collected from EPFL. Another IMAGE_PROCESSING is the handmade design to implement multiple modes of image transformations. We employ Synopsys Design Compiler 2019.12 with skywater 130nm technology library to produce the netlist and subsequently convert it into AIG by ABC (Brayton & Mishchenko, 2010).

Table 2: Validation dataset with different scale circuits.

name	#node	#edge	max level
small (avg.)	161.6	193.9	46
b12_opt_C	1,861	2,724	29
b14_opt_C	10,502	16,135	96
mem_ctrl	84,742	130,550	198
Image_Processing	402,193	506,340	27

We present the results for circuits of varying scales in Figure 7a and Figure 7b, from which we draw three key observations. First, GNNs struggle to perform well across circuits of varying scales, while transformer-based models, such as DeepGate3† and DeepGate4, exhibits superior performance on both functional and structural tasks, which suggests that global aggregation mechanism is crucial in circuit representation learning. Second, with our proposed partitioning method and updating strategy, both DeepGate3† and DeepGate4 exhibit strong generalizability. Despite being trained on circuits averaging 15K gates, the performance on the IMAGE_PROCESSING demonstrates DeepGate3† and DeepGate4 maintain outstanding performance on OOD circuits. Last, DeepGate4 shows stable performance across circuits of different scales, with a standard deviation of 0.46 on overall loss. In contrast, GNNs show unstable performance, particularly in structural loss with a standard deviation of 4.38, as highlighted in Figure 7b.

Table 3: Comparison on ITC99 and EPFL Random Control Benchmark.

Method	ITC99					EPFL Random Control				
	Inference Stage		Performance			Inference Stage		Performance		
	Time(s)	Mem.(MB)	L_{func}	L_{stru}	L_{all}	Time(s)	Mem.(MB)	L_{func}	L_{stru}	L_{all}
GCN	0.297	415	1.04 ± 0.024	5.61 ± 0.478	6.65 ± 0.471	0.286	705	1.02 ± 0.028	21.16 ± 3.023	22.18 ± 3.002
GraphSAGE	0.020	415	0.90 ± 0.022	4.95 ± 0.403	5.85 ± 0.391	0.025	706	0.94 ± 0.014	5.94 ± 0.923	6.88 ± 0.937
GAT	0.029	415	1.15 ± 0.011	8.17 ± 1.111	9.32 ± 1.102	0.035	705	1.13 ± 0.020	14.46 ± 1.335	15.59 ± 1.351
PNA	0.042	423	0.85 ± 0.010	6.10 ± 2.062	6.95 ± 2.065	0.059	713	0.88 ± 0.010	10.10 ± 2.218	10.98 ± 2.213
DeepGate2	0.490	412	0.79 ± 0.002	5.49 ± 0.157	6.28 ± 0.158	0.470	694	0.90 ± 0.004	25.78 ± 1.546	26.69 ± 1.546
PolarGate	0.030	416	1.07 ± 0.014	4.62 ± 0.158	5.69 ± 0.162	0.033	707	1.06 ± 0.009	9.40 ± 2.863	10.45 ± 2.855
HOGA-5	0.290	1010	0.98 ± 0.002	6.02 ± 0.290	6.99 ± 0.291	0.648	2006	1.02 ± 0.004	6.33 ± 0.290	7.35 ± 0.293
GraphGPS†	0.512	480	0.78 ± 0.020	4.99 ± 0.172	5.77 ± 0.174	0.650	906	1.44 ± 0.018	11.15 ± 0.553	12.58 ± 0.553
Exphormer†	0.441	337	0.64 ± 0.002	3.86 ± 0.207	4.50 ± 0.207	0.661	117	0.85 ± 0.027	5.59 ± 0.566	6.43 ± 0.577
DAGformer†	0.676	1324	1.02 ± 0.003	5.99 ± 0.223	7.01 ± 0.223	0.886	292	1.33 ± 0.019	7.11 ± 0.100	8.43 ± 0.091
DeepGate3†	11.322	6565	0.53 ± 0.026	3.21 ± 0.152	3.73 ± 0.148	18.349	2730	1.16 ± 0.092	6.97 ± 0.630	8.13 ± 0.697
DeepGate4	2.496	479	**0.49 ± 0.002**	**2.68 ± 0.074**	**3.16 ± 0.076**	2.263	130	**0.79 ± 0.021**	**3.64 ± 0.583**	**4.43 ± 0.577**
Fused-DG4	1.463	233				1.624	91			

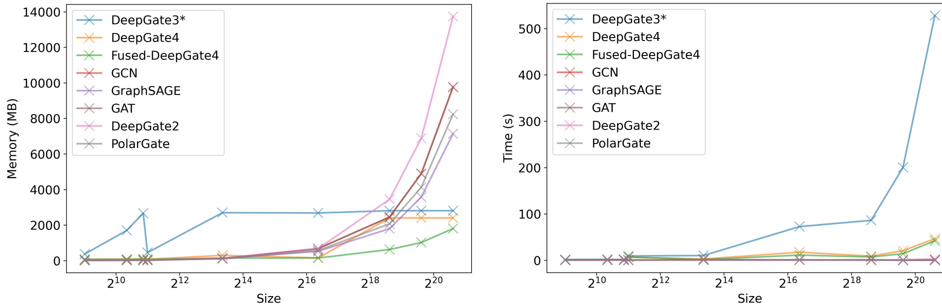

(a) Memory Consumption

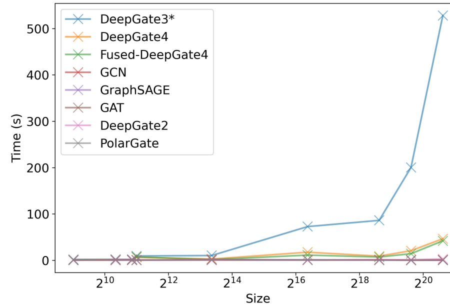

(b) Time Consumption

Figure 8: Inference resource usage over different scale circuits.

4.4 MEMORY&RUNTIME ANALYSIS

In this section, we discuss memory consumption and runtime when scaling to larger circuits. We evaluate all models on the EPFL dataset, as detailed in Table 6. For circuits larger than 400K gates, we extend the IMAGE_PROCESSING dataset in Table 2 by duplicating it 2 and 4 times to create circuits with 800K and 1.6M gates. During inference, we use a mini-batch size of 128, and drop all task heads, i.e. we use each model solely to compute embeddings.

Inference Memory Usage As shown in Figure 8a, for GNNs, memory usage increases linearly with graph size. For our models, memory consumption also scales linearly for small circuits. However, for circuits exceeding a certain size, the memory usage of our models stabilizes. This is primarily because, for smaller circuits, the cones within the same level are smaller than the mini-batch size. These results indicate that the memory consumption of our model is sub-linear with respect to graph size. Additionally, compared to DeepGate3†, DeepGate4 demonstrates a significant overall reduction in memory usage, with an overall 58.4% reduction. Fused-DeepGate4 further reduces memory usage by 78.5%.

Inference Runtime As shown in Figure 8b, the time consumption of all models scales linearly with graph size. Since our graph transformer models partition the original graph into cones and

encode them level by level, they are significantly slower than GNNs. To mitigate this, we introduce inference optimization, as described in Section 3.7. With these optimizations, our proposed Fused-DeepGate4 reduces time consumption by 90.5% and 18.5% compared to DeepGate3† and DeepGate4, respectively.

Table 4: Ablation Study on ITC99 and EPFL Random Control Benchmark

Method	ITC99					EPFL Random Control				
	Inference Stage		Performance			Inference Stage		Performance		
	Time(s)	Mem.(MB)	L_{func}	L_{stru}	L_{all}	Time(s)	Mem.(MB)	L_{func}	L_{stru}	L_{all}
w/o Mark	3.9223	1,060	**0.48** $\pm$ **0.004**	2.75 $\pm$ 0.041	3.23 $\pm$ 0.039	2.9906	182	0.90 $\pm$ 0.055	3.67 $\pm$ 0.689	4.58 $\pm$ 0.659
w/o Partition	-	OOM	-	-	-	-	OOM	-	-	-
w/o Balancer&SE	2.4591	479	0.50 $\pm$ 0.023	2.97 $\pm$ 0.060	3.47 $\pm$ 0.070	2.2085	130	0.82 $\pm$ 0.018	3.95 $\pm$ 0.847	4.77 $\pm$ 0.850
DeepGate3†	11.322	6565	0.53 $\pm$ 0.026	3.21 $\pm$ 0.152	3.73 $\pm$ 0.148	18.349	2730	1.16 $\pm$ 0.092	6.97 $\pm$ 0.630	8.13 $\pm$ 0.697
DeepGate4	2.496	479	0.49 $\pm$ 0.002	**2.68** $\pm$ **0.074**	**3.16** $\pm$ **0.076**	2.263	130	**0.79** $\pm$ **0.021**	**3.64** $\pm$ **0.583**	**4.43** $\pm$ **0.577**
Fused-DeepGate4	**1.463**	**233**				**1.624**	**91**			

4.5 Ablation Study

In this section, we perform ablation studies on the primary components of DeepGate4 following the metrics outlined in Section 3.6. All results are reported in Table 4.

Effect of Mark In the setting DeepGate4 without Mark (w/o Mark), not marking overlapping nodes between cones resulted in redundant computations and gradient updates. This increased average inference time and memory usage by 45.3% and 286.4%, respectively, compared to DeepGate4, demonstrating that the marking process significantly improves efficiency and reduces memory consumption without a large impact on the loss.

Effect of Partition Partitioning played a critical role, especially with large circuit datasets that contain a large amount of nodes. In the setting DeepGate4 without partitioning (w/o Partition), the model encounters OOM errors on both ITC99 and EPFL, highlighting the necessity of partitioning for memory usage reduction.

Effect of Sparse Transformer After partitioning, the inherent connectivity and sparsity in each cone allowed replacing the transformer in DeepGate3 with a sparse transformer. DeepGate4 significantly improved speed and memory efficiency, reducing inference time by 84.0% on average and reducing memory usage by 93.4% compared to the DeepGate3†.

Effect of Loss Balancer&Structural Encoding The introduction of the Loss Balancer and structural encoding has almost no impact on inference time and memory usage, while significantly reducing losses, particularly the structural loss. On the two benchmarks, DeepGate4 achieved reductions of 3.38%, 8.75%, and 7.89% in functional, structural, and overall loss, respectively, compared to DeepGate4 without Loss Balancer and Structural Encoding (w/o Balancer&SE).

Effect of Fused-DeepGate4 By introducing the SOTA GAT acceleration method, Fused-GAT, and our customized Fused-DG2 tailored specifically for the characteristics of AIGs, we further reduced both runtime and memory consumption. Compared to DeepGate4, Fused-DeepGate4 achieved an average reduction of 35.1% in inference time, and 46.8% in memory usage.

5 Conclusion

In this paper, we propose DeepGate4, an efficient and scalable representation learning model capable of handling large circuits with millions or even billions of gates. DeepGate4 introduces a novel partitioning method and update strategy applicable to any graph transformers. Additionally, it leverages a GAT-based sparse transformer with inference acceleration optimization, termed Fused-DeepGate4, specifically tailored for AIGs. Our model further incorporates global and local structural encodings, along with a loss balancer that automatically adjusts the weights of multitask losses. Experimental results on the ITC99 and EPFL benchmarks demonstrate that DeepGate4 significantly outperforms state-of-the-art methods. Moreover, the Fused-DeepGate4 variant achieves substantial reductions in both runtime and memory usage, further enhancing efficiency.

540 541 542 543 544 545 546 547 548 549 550 551 552 553 554 555 556 557 558 559 560 561 562 563 564 565 566 567 568 569 570 571 572 573 574 575 576 577 578 579 580 581 582 583 584 585 586 587 588 589 590 591 592 593

REFERENCES

Singh Akansha. Over-squashing in graph neural networks: A comprehensive survey. *arXiv preprint arXiv:2308.15568*, 2023.

Uri Alon and Eran Yahav. On the bottleneck of graph neural networks and its practical implications. *arXiv preprint arXiv:2006.05205*, 2020.

Luca Amarú, Pierre-Emmanuel Gaillardon, and Giovanni De Micheli. The epfl combinational benchmark suite. In *IWLS*, number CONF, 2015.

Robert Brayton and Alan Mishchenko. Abc: An academic industrial-strength verification tool. In *CAV 2010, Edinburgh, UK, July 15-19, 2010. Proceedings 22*, pp. 24–40. Springer, 2010.

Horst Bunke. On a relation between graph edit distance and maximum common subgraph. *Pattern recognition letters*, 18(8):689–694, 1997.

Jinsong Chen, Kaiyuan Gao, Gaichao Li, and Kun He. Nagphormer: A tokenized graph transformer for node classification in large graphs. *arXiv preprint arXiv:2206.04910*, 2022.

Zhao Chen, Vijay Badrinarayanan, Chen-Yu Lee, and Andrew Rabinovich. Gradnorm: Gradient normalization for adaptive loss balancing in deep multitask networks. In *International conference on machine learning*, pp. 794–803. PMLR, 2018.

Zhaodong Chen, Mingyu Yan, Maohua Zhu, Lei Deng, Guoqi Li, Shuangchen Li, and Yuan Xie. fusegnn: Accelerating graph convolutional neural network training on gpgpu. In *Proceedings of the 39th International Conference on Computer-Aided Design*, pp. 1–9, 2020.

Animesh Basak Chowdhury, Benjamin Tan, Ramesh Karri, and Siddharth Garg. Openabc-d: A large-scale dataset for machine learning guided integrated circuit synthesis, 2021.

Gabriele Corso, Luca Cavalleri, Dominique Beaini, Pietro Liò, and Petar Veličković. Principal neighbourhood aggregation for graph nets. *Advances in Neural Information Processing Systems*, 33:13260–13271, 2020.

Scott Davidson. Characteristics of the itc'99 benchmark circuits. In *ITSW*, 1999.

Alexandre Défossez, Jade Copet, Gabriel Synnaeve, and Yossi Adi. High fidelity neural audio compression. *arXiv preprint arXiv:2210.13438*, 2022.

Chenhui Deng, Zichao Yue, Cunxi Yu, Gokce Sarar, Ryan Carey, Rajeev Jain, and Zhiru Zhang. Less is more: Hop-wise graph attention for scalable and generalizable learning on circuits. *arXiv preprint arXiv:2403.01317*, 2024.

Mucong Ding, Tahseen Rabbani, Bang An, Evan Wang, and Furong Huang. Sketch-gnn: Scalable graph neural networks with sublinear training complexity. *Advances in Neural Information Processing Systems*, 35:2930–2943, 2022.

Nicole Eikmeier and David F Gleich. Revisiting power-law distributions in spectra of real world networks. In *Proceedings of the 23rd ACM SIGKDD international conference on knowledge discovery and data mining*, pp. 817–826, 2017.

Matthias Fey, Jan E Lenssen, Frank Weichert, and Jure Leskovec. Gnnautoscale: Scalable and expressive graph neural networks via historical embeddings. In *International conference on machine learning*, pp. 3294–3304. PMLR, 2021.

Will Hamilton, Zhitao Ying, and Jure Leskovec. Inductive representation learning on large graphs. *Advances in neural information processing systems*, 30, 2017.

Sadaf Khan, Zhengyuan Shi, Min Li, and Qiang Xu. Deepseq: Deep sequential circuit learning. *arXiv preprint arXiv:2302.13608*, 2023.

Thomas N Kipf and Max Welling. Semi-supervised classification with graph convolutional networks. *arXiv preprint arXiv:1609.02907*, 2016.

594 595 596 597 598 599 600 601 602 603 604 605 606 607 608 609 610 611 612 613 614 615 616 617 618 619 620 621 622 623 624 625 626 627 628 629 630 631 632 633 634 635 636 637 638 639 640 641 642 643 644 645 646 647

Devin Kreuzer, Dominique Beaini, Will Hamilton, Vincent Létourneau, and Prudencio Tossou. Rethinking graph transformers with spectral attention. *Advances in Neural Information Processing Systems*, 34:21618–21629, 2021.

Min Li, Sadaf Khan, Zhengyuan Shi, Naixing Wang, Huang Yu, and Qiang Xu. Deepgate: Learning neural representations of logic gates. In *Proceedings of the 59th ACM/IEEE Design Automation Conference*, pp. 667–672, 2022.

Min Li, Zhengyuan Shi, Qiuxia Lai, Sadaf Khan, Shaowei Cai, and Qiang Xu. On eda-driven learning for sat solving. In *2023 60th ACM/IEEE Design Automation Conference (DAC)*. IEEE, 2023.

Jiawei Liu, Jianwang Zhai, Mingyu Zhao, Zhe Lin, Bei Yu, and Chuan Shi. Polargate: Breaking the functionality representation bottleneck of and-inverter graph neural network. In *2024 IEEE/ACM International Conference on Computer-Aided Design (ICCAD)*, 2024.

Yuankai Luo, Veronika Thost, and Lei Shi. Transformers over directed acyclic graphs. *Advances in Neural Information Processing Systems*, 36, 2024.

Grégoire Mialon, Dexiong Chen, Margot Selosse, and Julien Mairal. Graphit: Encoding graph structure in transformers. *arXiv preprint arXiv:2106.05667*, 2021.

PyG. Pytorch geometric, 2024. `https://www.pyg.org/`.

SEPARATE DECISION QUEUE. Cadical at the sat race 2019. *SAT RACE 2019*, pp. 8, 2019.

Ladislav Rampášek, Michael Galkin, Vijay Prakash Dwivedi, Anh Tuan Luu, Guy Wolf, and Dominique Beaini. Recipe for a general, powerful, scalable graph transformer. *Advances in Neural Information Processing Systems*, 35:14501–14515, 2022.

T Konstantin Rusch, Michael M Bronstein, and Siddhartha Mishra. A survey on oversmoothing in graph neural networks. *arXiv preprint arXiv:2303.10993*, 2023.

Zhengyuan Shi, Min Li, Sadaf Khan, Liuzheng Wang, Naixing Wang, Yu Huang, and Qiang Xu. Deeptpi: Test point insertion with deep reinforcement learning. In *2022 IEEE International Test Conference (ITC)*, pp. 194–203. IEEE, 2022.

Zhengyuan Shi, Hongyang Pan, Sadaf Khan, Min Li, Yi Liu, Junhua Huang, Hui-Ling Zhen, Mingxuan Yuan, Zhufei Chu, and Qiang Xu. Deepgate2: Functionality-aware circuit representation learning. In *2023 IEEE/ACM International Conference on Computer Aided Design*. IEEE, 2023.

Zhengyuan Shi, Tiebing Tang, Sadaf Khan, Hui-Ling Zhen, Mingxuan Yuan, Zhufei Chu, and Qiang Xu. Eda-driven preprocessing for sat solving. *arXiv preprint arXiv:2403.19446*, 2024a.

Zhengyuan Shi, Ziyang Zheng, Sadaf Khan, Jianyuan Zhong, Min Li, and Qiang Xu. Deepgate3: Towards scalable circuit representation learning. *arXiv preprint arXiv:2407.11095*, 2024b.

Hamed Shirzad, Ameya Velingker, Balaji Venkatachalam, Danica J Sutherland, and Ali Kemal Sinop. Exphormer: Sparse transformers for graphs. In *International Conference on Machine Learning*, pp. 31613–31632. PMLR, 2023.

Petar Veličković, Guillem Cucurull, Arantxa Casanova, Adriana Romero, Pietro Lio, and Yoshua Bengio. Graph attention networks. *arXiv preprint arXiv:1710.10903*, 2017.

Nan Wu, Yingjie Li, Cong Hao, Steve Dai, Cunxi Yu, and Yuan Xie. Gamora: Graph learning based symbolic reasoning for large-scale boolean networks. In *2023 60th ACM/IEEE Design Automation Conference (DAC)*. IEEE, 2023.

Qitian Wu, Wentao Zhao, Zenan Li, David P Wipf, and Junchi Yan. Nodeformer: A scalable graph structure learning transformer for node classification. *Advances in Neural Information Processing Systems*, 35:27387–27401, 2022.

Chengxuan Ying, Tianle Cai, Shengjie Luo, Shuxin Zheng, Guolin Ke, Di He, Yanming Shen, and Tie-Yan Liu. Do transformers really perform badly for graph representation? *Advances in neural information processing systems*, 34:28877–28888, 2021.

Haiyang Yu, Limei Wang, Bokun Wang, Meng Liu, Tianbao Yang, and Shuiwang Ji. Graphfm: Improving large-scale gnn training via feature momentum. In *International Conference on Machine Learning*, pp. 25684–25701. PMLR, 2022.

Hengrui Zhang, Zhongming Yu, Guohao Dai, Guyue Huang, Yufei Ding, Yuan Xie, and Yu Wang. Understanding gnn computational graph: A coordinated computation, io, and memory perspective. *Proceedings of Machine Learning and Systems*, 4:467–484, 2022.

A APPENDIX

A.1 DATASET STATISTIC

Table 5: ITC99 Dataset

split	name	#node	#edge	#PI	#PO	max level	#cones
train	b07_opt_C	718	1029	50	49	48	121
	b17_opt_C	47652	73743	1451	1442	104	8457
	b02_opt_C	47	65	4	4	9	6
	b09_opt_C	285	391	29	28	20	48
	b05_opt_C	956	1428	35	55	67	166
	b15_opt_C	14611	22542	485	449	95	2548
	b20_opt_C	23788	36709	522	508	102	4083
	b13_opt_C	538	720	62	53	23	75
	b11_opt_C	999	1487	38	31	56	134
	b01_opt_C	79	113	5	4	10	8
	b03_opt_C	276	371	34	28	19	52
	b06_opt_C	81	117	5	8	10	10
	b04_opt_C	1105	1554	77	64	51	180
	b18_opt_C	140638	217943	3306	3282	214	23214
	b22_opt_C	34035	52319	735	719	103	6133
	b10_opt_C	337	486	28	17	19	54
	b08_opt_C	306	422	30	21	24	40
	b21_opt_C	23888	36867	522	508	100	4403
val	b12_opt_C	1861	2724	126	117	29	328
	b14_opt_C	10502	16135	275	243	96	1751
Avg	-	15135.1	23358.25	390.95	381.5	59.95	2590.55

Table 6: EPFL Random Control Dataset

split	name	#node	#edge	#PI	#PO	max level	#cones
train	router	519	716	60	3	72	72
	i2c	2378	3584	136	127	36	311
	int2float	458	707	11	7	31	44
	mem_ctrl	84742	130550	1028	941	198	14234
	voter	27721	40478	1001	1	136	3822
	ctrl	328	495	7	25	19	64
	priority	2043	2893	128	8	498	262
	dec	320	616	8	256	4	256
val	cavlc	1298	1981	10	11	32	146
	arbiter	23488	35071	256	129	174	3714
Avg	-	14329.5	21709.1	264.5	150.8	120	2292.5

756
757
758
759
760
761
762
763
764
765
766
767
768
769
770
771
772
773
774
775
776
777
778
779
780
781
782
783
784
785
786
787
788
789
790
791
792
793
794
795
796
797
798
799
800
801
802
803
804
805
806
807
808
809

Table 7: OpenABC-D Dataset

split	name	#node	#edge	#PI	#PO	max level	#cones
train	spi	8565	12530	254	238	69	1348
	i2c	2195	3187	177	128	27	291
	ss_pcm	866	1165	104	90	13	144
	usb_phy	1025	1380	132	85	16	143
	sasc	1349	1827	135	124	15	165
	wb_dma	9059	12818	828	660	41	1779
	simple_spi	1928	2694	164	132	23	316
	pci	41708	57826	3429	3131	52	6439
	dynamic_node	36469	51855	2708	2560	55	5170
	ac97_ctrl	24399	33524	2339	2130	19	3568
	mem_ctrl	31001	47906	1187	937	56	3949
	des3_area	8069	12737	303	32	47	1226
	aes	39898	68140	683	529	44	4734
	sha256	30634	44507	1943	1042	143	4606
	fir	9412	13560	410	319	86	1526
	iir	14139	20623	494	404	131	2377
	idft	518787	722736	37603	37383	82	90525
	tv80	19877	30569	636	361	99	3025
	fpu	56567	85558	632	339	1522	8986
	aes_xcrypt	67660	111525	1975	1682	76	11490
	jpeg	233573	343382	4962	4789	75	33429
	tinyRocket	104336	152090	4561	4094	156	17548
	picosoc	173744	245387	11302	10786	75	30211
	vga_lcd	226448	314460	17322	17049	44	43939
val	dft	525762	733211	37597	37382	83	91763
	wb_conmax	83229	128947	2122	2032	35	12002
	ethernet	143316	199749	10731	10401	59	25661
	bp_be	171292	242214	11592	8225	150	25092
	aes_secworks	74990	112681	3087	2603	71	12420
Avg	-	91734.38	131337.5	5496.966	5160.931	116	15305.93

A.2 Training Objective

The DeepGate4 model is trained on multiple tasks at both the gate-level and graph-level. To disentangle the functional and structural embeddings, we design training tasks with distinct labels to supervise each component.

Gate-level Tasks. For function-related tasks at the gate-level, we incorporate the training tasks from DeepGate2, which involve predicting the logic-1 probability of gates and the pair-wise truth table distance. We sample gate pairs, $\mathcal{N}_{gate_tt}$, and record their corresponding simulation responses as incomplete truth tables, T_i. The pair-wise truth table distance D^{gate_tt} is computed as follows:

$$D^{gate_tt}_{(i,j)} = \frac{HammingDistance(T_i, T_j)}{length(T_i)}, (i,j) \in \mathcal{N}_{gate_tt} \tag{6}$$

The loss functions for gate-level functional tasks are:

$$\begin{aligned} L^{prob}_{gate} &= L1Loss(p_k, MLP_{prob}(hf_k)), k \in \mathcal{V} \\ L^{tt_pair}_{gate} &= L1Loss(D^{gate_tt}_{(i,j)}, MLP_{gate_tt}(hf_i, hf_j)), (i,j) \in \mathcal{N}_{gate_tt} \end{aligned} \tag{7}$$

In addition, we incorporate supervision for structural learning by predicting pair-wise connections. Since DeepGate4 encodes the logic level as part of the structural encoding, we drop the task of predicting logic levels. The prediction of pair-wise connections is treated as a classification task,

where a sampled gate pair $(i, j) \in \mathcal{N}_{gate_con}$ can be classified into two categories: (1) there exists a path from i to j or from j to i, or (2) otherwise. The loss function is defined as follows:

$$L_{gate}^{con} = BCELoss(MLP_{con}(hs_i, hs_j)), (i, j) \in \mathcal{N}_{gate_con} \tag{8}$$

Graph-level Tasks. For each sub-graph, we perform a complete simulation to prepare the truth table, denoted as T_s. Additionally, we collect two structural characteristics for each sub-graph: the number of nodes $Size(s)$ and the depth $Depth(s)$. After obtaining the functional embedding hf^s and structural embedding hs^s via pooling in the Transformer, the following loss functions supervise the training, where $s \in \mathcal{S}$:

$$\begin{aligned} L_{graph}^{size} &= L1Loss(Size(s), MLP_{size}(hs^s)) \\ L_{graph}^{depth} &= L1Loss(Depth(s), MLP_{depth}(hs^s)) \\ L_{graph}^{tt} &= BCELoss(T_s, MLP_{tt}(hf^s)) \end{aligned} \tag{9}$$

We also introduce loss functions to capture pair-wise correlations between sub-graphs. The truth table distance $D_{(s_1,s_2)}^{graph_tt}$ and graph edit distance (Bunke, 1997) $D_{(s_1,s_2)}^{graph_ged}$ between two sub-graphs (s_1, s_2) are predicted using the following formulas:

$$\begin{aligned} D_{(s_1,s_2)}^{graph_tt} &= \frac{HammingDistance(T_{s_1}, T_{s_2})}{length(T_{s_1})} \\ L_{graph}^{tt_pair} &= L1Loss(D_{(s_1,s_2)}^{graph_tt}, MLP_{graph_tt}(hf^{s_1}, hf^{s_2})) \\ D_{(s_1,s_2)}^{graph_ged} &= GraphEditDistance(s_1, s_2) \\ L_{graph}^{ged_pair} &= L1Loss(D_{(s_1,s_2)}^{graph_ged}, MLP_{graph_ged}(hs^{s_1}, hs^{s_2})) \end{aligned} \tag{10}$$

To link the gate-level and graph-level embeddings, we enable the model to predict whether gate k belongs to sub-graph s using the structural embeddings. The loss function is defined as:

$$L_{in} = BCELoss(\{0, 1\}, MLP_{in}(hs_k, hs^s)) \tag{11}$$

Error of Truth Table Prediction. For each 6-input sub-graph s in the test dataset $\mathcal{S}'$, we predict the 64-bit truth table based on the graph-level functional embedding hf^s. The prediction error is calculated by the Hamming distance between the prediction and ground truth:

$$P^{tt} = \frac{1}{len(\mathcal{S}')} \sum_{s}^{\mathcal{S}'} HammingDistance(T_s, MLP_{tt}(hf^s)) \tag{12}$$

Accuracy of Gate Connection Prediction. Given the structural embedding of the gate pair (i, j) in the test dataset $\mathcal{N}'_{con}$ and the binary label $y_{(i,j)}^{con} = \{0, 1\}$, we define the accuracy of gate connection prediction as:

$$P^{con} = \frac{1}{len(\mathcal{N}'_{con})} \sum_{(i,j)}^{\mathcal{N}'_{con}} \mathbb{1}(y_{(i,j)}^{con}, MLP_{con}(hs_i, hs_j)) \tag{13}$$

Accuracy of Gate-in-Graph Prediction. For each gate-graph pair (k, s) in the test dataset $\mathcal{N}'_{in}$, we predict whether the gate is included in the sub-graph based on the gate structural embedding hs_k and the sub-graph structural embedding hs^s. The binary label is $y_{(k,s)}^{in} = \{0, 1\}$. The accuracy is defined as:

$$P^{in} = \frac{1}{len(\mathcal{N}'_{in})} \sum_{(k,s)}^{\mathcal{N}'_{in}} \mathbb{1}(MLP_{in}(hs_k, hs^s), y_k^{in}) \tag{14}$$

864
865
866
867
868
869
870
871
872
873
874
875
876
877
878
879
880
881
882
883
884
885
886
887
888
889
890
891
892
893
894
895
896
897
898
899
900
901
902
903
904
905
906
907
908
909
910
911
912
913
914
915
916
917

A.3 Ablation Study on Graph Partition Hyperparameters

In this section, we include a detailed analysis of the hyperparameters k and δ. In our graph partition algorithm, k denotes the maximum level of the cone, and δ denotes the stride. These parameters influence memory usage and overlap levels as follows:

- k (Maximum Level): k determines the upper bound of the subgraph size. Specifically, the size of a subgraph is always smaller than $2^{k+1} - 1$. Larger subgraphs require more GPU memory; for example, with the same mini-batch size, increasing k significantly increases memory consumption.
- δ (Stride): δ determines the overlap region between subgraphs. The overlap level is defined as $k - \delta + 1$, which directly influences the inter-level message-passing ratio.

Furthermore, we provide an ablation study on k and δ, illustrating the sensitivity of our model to these hyperparameters. As shown in Table 8, we conclude two observations from the ablation study. First, settings such as $(k = 8, \delta = 8)$, $(k = 8, \delta = 6)$, and $(k = 8, \delta = 4)$ demonstrate that our method is not sensitive to overlap ratios, as performance across these settings is similar. Second, settings such as $(k = 8, \delta = 6)$, $(k = 10, \delta = 8)$, and $(k = 6, \delta = 4)$ maintain the same overlap level but vary in subgraph size. Results demonstrate that increasing k significantly impacts GPU memory usage. Furthermore, larger k will degrade structural task performance. This is because structural tasks rely more heavily on local information, especially for metrics like $L_{graph}^{ged_pair}$, L_{graph}^{size}, and L_{graph}^{depth} (See Section A.2).

Table 8: Ablation Study on k and δ

Setting		Metric			
k	δ	Train Mem.	L_{func}	L_{stru}	L_{all}
8	8	12.62GB	0.4649 ± 0.0017	2.4519 ± 0.0625	2.9168 ± 0.0639
8	6	12.62GB	0.4863 ± 0.0023	2.6783 ± 0.0739	3.1646 ± 0.0761
8	4	12.62GB	0.4713 ± 0.0034	2.5821 ± 0.0963	3.0534 ± 0.0933
10	8	33.90GB	0.4638 ± 0.0108	3.2055 ± 0.0747	3.6692 ± 0.0760
6	4	6.59GB	0.4629 ± 0.0065	2.6563 ± 0.0587	3.1192 ± 0.0567

A.4 Comparsion on OpenABC-D

Implementation Details We collect the circuits from OpenABC-D (Chowdhury et al., 2021). All designs are transformed into AIGs by ABC tool (Brayton & Mishchenko, 2010). The statistical details of datasets can be found in Section A.1. We follow the experiment setting in Section 4.1. All experiments are performed on one L40 GPU with 48GB maximum memory. For training objectives, we use the gate-level tasks in Section A.2.

Comparison on Effectiveness DeepGate4 demonstrates outstanding effectiveness across all training tasks. As shown in Table 9, it achieves state-of-the-art performance on all gate-level tasks within

Table 9: Comparsion on OpenABC-D benchmark.

Model	Param.	Mem.	L_{gate}^{prob}	$L_{gate}^{tt_pair}$	L_{gate}^{con}	P^{con}	L_{all}
GCN	0.76M	19.72G	0.1600 ± 0.0484	0.1168 ± 0.0270	0.6926 ± 0.0808	$59.93\% \pm 5.89\%$	0.9695 ± 0.1168
GraphSAGE	0.89M	23.23G	0.0607 ± 0.0044	0.0745 ± 0.0063	0.6651 ± 0.0458	$64.25\% \pm 3.27\%$	0.8004 ± 0.0453
GAT	0.76M	33.02G	0.2036 ± 0.0142	0.1040 ± 0.0130	0.6293 ± 0.0178	$64.94\% \pm 1.87\%$	0.9370 ± 0.0283
PNA	2.75M	OOM	-	-	-	-	-
DeepGate2	1.28M	24.15G	0.0406 ± 0.0004	0.0621 ± 0.0003	0.6976 ± 0.0079	$63.16\% \pm 0.77\%$	0.8003 ± 0.0083
DeepGate3	8.17M	OOM	-	-	-	-	-
PolarGate	0.88M	44.48G	0.7767 ± 0.3965	0.1179 ± 0.0615	0.9096 ± 0.1934	$53.00\% \pm 14.82\%$	1.8042 ± 0.3771
HOGA-2	0.78M	43.12G	0.1635 ± 0.0004	0.0896 ± 0.0002	0.6245 ± 0.0004	$64.81\% \pm 0.42\%$	0.8777 ± 0.0005
HOGA-5	0.78M	OOM	-	-	-	-	-
DeepGate4	7.37M	41.09G	$\mathbf{0.0233 \pm 0.0010}$	$\mathbf{0.0462 \pm 0.0019}$	$\mathbf{0.4789 \pm 0.0180}$	$\mathbf{79.00\% \pm 0.30\%}$	$\mathbf{0.5484 \pm 0.0166}$

918 the OpenABC-D datasets. Notably, DeepGate4 reduces the overall loss by 31.48% compared to the second-best method. Moreover, while baseline models struggle with gate connection prediction, DeepGate4 significantly enhances performance in this area, achieving an accuracy of 79%. This highlights the outstanding ability of DeepGate4 to capture the structural relationships between gates.

Comparison on Efficiency In terms of efficiency, models like PNA and HOGA-5 encounter out-of-memory (OOM) errors, whereas DeepGate4 can successfully train a graph transformer on large circuits containing over 500k gates.

A.5 LOGIC EQUIVALENCE CHECKING

Logic Equivalence Checking (LEC) is a critical task in Formal Verification, aimed at determining whether two designs are functionally equivalent. As circuit complexity grows, the significance of LEC increases since design errors in such systems can lead to costly fixes or operational failures in the final product.

We evaluate LEC on the ITC99 dataset by extracting subcircuits with multiple primary inputs (PIs) and a single primary output (PO). Given a subcircuit pair (G_1, G_2), the model performs a binary classification task to predict whether G_1 and G_2 are equivalent. In the candidate pairs, only 1.29% of pairs are equivalent, highlighting the challenge of imbalanced data. To assess performance, we use the widely adopted metrics Average Precision (AP) and Precision-Recall Area Under the Curve (PR-AUC). These metrics are threshold-independent and particularly effective for imbalanced datasets, where one class is significantly rarer than the other.

Table 10: Logic Equivalence Checking

Method	AP	PR-AUC
GCN	0.05	0.04
GraphSAGE	0.10	0.11
GAT	0.02	0.02
PNA	0.20	0.17
HOGA-5	0.03	0.03
DeepGate2	0.13	0.13
PolarGate	0.03	0.21
DeepGate3	OOM	OOM
DeepGate3†	0.17	0.17
DeepGate4	**0.31**	**0.30**

Note that DeepGate3† denotes that we use our proposed updating strategy and training pipline. As shown in Table 10, DeepGate4 outperforms all other methods by a significant margin, achieving the highest AP (0.31) and PR-AUC (0.30), and improve these two metrics by 55% and 42% respectively, compared to the second-best method. These values indicate its superior ability to balance precision and recall, especially in scenarios with imbalanced data.

A.6 BOOLEAN SATISFIABILITY PROBLEM

The Boolean Satisfiability (SAT) problem is a fundamental computational problem that determines whether a Boolean formula can evaluate to logic-1 for at least one variable assignment. As the first proven NP-complete problem, SAT serves as a cornerstone in computer science, with applications spanning fields such as scheduling, planning, and verification. Modern SAT solvers primarily utilize the conflict-driven clause learning (CDCL) algorithm, which efficiently handles path conflicts during the search process and explores additional constraints to reduce the search space. Over the years, various heuristic strategies have been developed to further accelerate CDCL in SAT solvers.

We follow the setting in DeepGate2 (Shi et al., 2023). We utilize the CaDiCal (QUEUE, 2019) SAT

Table 11: SAT solving time comparsion.† denotes that we use our updating strategy.

Case	Name	ad44	f20	ab18	ac1	ad14	Avg.
	Size	44949	27806	37275	42038	44949	39403.4
Baseline	Solving Time	918.21	1046.31	3150.81	5522.85	5766.85	3281.01
DeepGate3†	Model Runtime	27.73	16.57	22.60	33.17	27.27	25.47
	Solving Time	678.42	952.91	1607.06	6189.61	4413.96	2768.39
PolarGate	Model Runtime	0.01	0.01	0.01	0.24	0.01	0.06
	Solving Time	**606.74**	1154.87	**1000.02**	3923.88	**3222.98**	1981.70
Exphormer†	Model Runtime	0.74	0.51	0.62	0.64	0.97	0.70
	Solving Time	885.98	1177.07	1293.57	4156.04	3387.24	2179.98
DeepGate4	Model Runtime	3.65	2.80	3.10	3.33	3.62	3.30
	Solving Time	970.28	**143.09**	1351.49	**393.25**	4268.57	**1425.34**

solver as the backbone solver and modify the variable decision heuristic based on it. In the Baseline setting, SAT problems are directly solved using the backbone SAT solver. For model-acclerated SAT solving, given a SAT instance, the first step is to encode the corresponding AIG to get the gate embedding. During the variable decision process, a decision value d_i is assigned to variable v_i. If another variable v_j with an assigned value d_j is identified as correlated to v_i, the reversed value d_j' is assigned to v_i, i.e., $d_i = 0 \ if \ d_j = 1$ or $d_i = 1 \ if \ d_j = 0$. The determination of correlated variables relies on their functional similarity, and the similarity $Sim(v_i, v_j)$ exceeding the threshold θ indicates correlation.

The results are shown in Table 11. Since SAT solving is time-consuming, we compare our approach only with the top-3 methods listed in Table 1, namely DeepGate3†, Exphormer†, and PolarGate. The Baseline represents using the SAT solver without any model-based acceleration. Leveraging its exceptional ability to understand the functional relationships within circuits, DeepGate4 achieves a substantial reduction in SAT solving time, with an 86.33% reduction for case *f20* and an 92.90% reduction for case *ac1*. Regarding average solving time, it achieves a 56.56% reduction, outperforming all other methods. These results highlight DeepGate4's strong generalization capability and effectiveness in addressing real-world SAT solving challenges.